



Cite this: DOI: 10.1039/d1ta03161a

Ternary copolymers containing 3,4-dicyanothiophene for efficient organic solar cells with reduced energy loss†

Yue Zhang,^a Langheng Pan,^a Zhongxiang Peng,^c Wanyuan Deng,^a Bo Zhang,^{ab} Xiyue Yuan,^a Zhili Chen,^{ab} Long Ye,^{id c} Hongbin Wu,^{id a} Xiang Gao,^{*b} Zhitian Liu,^{*b} Chunhui Duan,^{id *a} Fei Huang^{id a} and Yong Cao^a

The power conversion efficiencies (PCEs) of organic solar cells (OSCs) based on non-fullerene acceptors are still limited by large energy loss (ΔE_{loss}). Herein, we report an easy and feasible way to reduce the ΔE_{loss} , specifically the energy losses caused by non-radiative recombination of OSCs via introducing 3,4-dicyanothiophene (DCT), a structurally simple building block with strong electron-withdrawing ability, into a state-of-the-art donor polymer PBDB-TF to form ternary copolymers. The effects of DCT content in the ternary copolymers on the optical properties, energy levels, film morphology, charge transport, photovoltaic performance, and energy losses are studied comprehensively. Significant efficiency improvement in OSCs has been achieved by the DCT-based ternary copolymers as compared to the benchmark polymer PBDB-TF mainly because of a higher open-circuit voltage enabled by the reduced non-radiative recombination energy loss. A high PCE of 16.6% and a low non-radiative recombination energy loss (0.22 eV) were achieved in ternary OSCs with the DCT-based terpolymer as the electron donor and Y6-BO and PC₇₁BM as the electron acceptors.

Received 15th April 2021

Accepted 1st June 2021

DOI: 10.1039/d1ta03161a

rsc.li/materials-a

Introduction

Organic solar cells (OSCs) have attracted much attention due to their light-weight, flexibility, semitransparency, and prospect in building-integrated photovoltaics.^{1–4} The emergence of small molecular non-fullerene acceptors (NFAs),^{5–8} the development of donor materials,^{9–13} and the progresses in device optimization^{14–16} and device physics studies^{17–20} contributed to the rapid increase of the power conversion efficiency (PCE) of OSCs. To date, the highest PCE of single-junction OSCs has exceeded 18%.^{10,21,22} But the PCE of OSCs still lags behind crystalline silicon and perovskite solar cells.²³ One of the main reasons is the relatively large energy loss (ΔE_{loss}) in OSCs.^{24–27} The ΔE_{loss} consists of three parts: radiative loss above bandgap ΔE_1 , radiative loss below bandgap ΔE_2 , and nonradiative loss ΔE_3 . The value of ΔE_1 depends on the bandgap and varies between 0.25 and 0.30 eV.²⁸ ΔE_2 can be as low as 50 meV in OSCs with

negligible energetic offsets,²⁹ which is comparable to crystalline silicon and perovskite solar cells.³⁰ However, the ΔE_3 is typically much larger than 0.2 eV in OSCs,^{31–33} which is larger than that of crystalline silicon and perovskite solar cells (where ΔE_3 can be lower than 0.1 eV).^{34,35} Hence, it is vital to suppress the non-radiation recombination to reduce the overall ΔE_{loss} .

The non-radiative recombination loss ΔE_3 can be calculated from $\Delta E_3 = -kT \ln(\text{EQE}_{\text{EL}})$, where k is Boltzmann constant, and T is the absolute temperature. Therefore, reducing the non-radiative recombination energy loss of an OSC means increasing the external quantum efficiency of electroluminescence (EQE_{EL}). The low EQE_{EL} in OSCs can be assigned to the existence of the interfacial CT state, formed at the interface between the donor and acceptor in the active layer.^{24,25} Smaller $\Delta V_{\text{oc}}^{\text{non-rad}}$ is usually found in materials systems with higher charge transfer state (E_{CT}).^{24,25,36} Therefore, it is necessary to upshift the lowest unoccupied molecular orbital (LUMO) levels of electron acceptors and/or downshift the highest occupied molecular orbital (HOMO) levels of electron donors.^{31–33,37,38} For example, Hou *et al.* developed a non-fullerene acceptor ITCCM-O with a wide bandgap of 2.0 eV.³⁹ The LUMO–LUMO offset between the polymer donor J52 and the acceptor ITCCM-O is only 0.09 eV, which enabled a remarkable high V_{oc} (1.34 V) and a very low ΔE_3 (0.22 eV). However, the absorption spectra will be blue-shifted when the LUMO levels of electron acceptors are elevated, which will cause reduced short-circuit current density (J_{sc}) of the resulting OSCs. Therefore, a more feasible strategy is

^aInstitute of Polymer Optoelectronic Materials and Devices, State Key Laboratory of Luminescent Materials and Devices, South China University of Technology, Guangzhou 510640, China. E-mail: duanchunhui@scut.edu.cn

^bHubei Engineering Technology Research Center of Optoelectronic and New Energy Materials, Wuhan Institute of Technology, Wuhan, 430205, China. E-mail: xgao@wit.edu.cn; able.ztliu@wit.edu.cn

^cSchool of Materials Science and Engineering, Tianjin University, Tianjin 300350, P. R. China

† Electronic supplementary information (ESI) available. See DOI: 10.1039/d1ta03161a

to downshift the HOMO level of electron donors. It has been reported that efficient exciton dissociation can occur at extremely small energy-level offsets, which leave sufficiently large room for energy level control to reduce E_{loss} of OSCs.^{40–43}

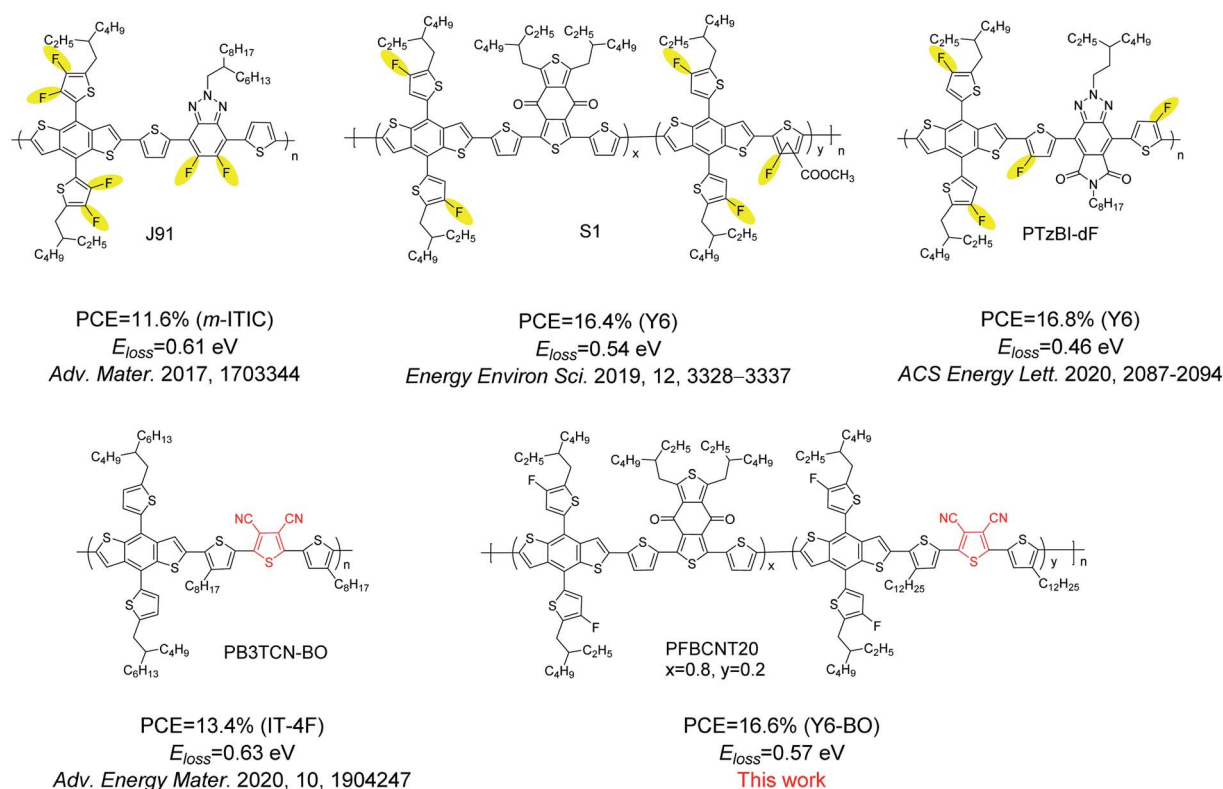
Polymer donors for high-efficiency OSCs are mainly copolymers based on benzo-[1,2-*b*:4,5-*b'*]dithiophene (BDT) and various acceptor units. Electron-withdrawing substituents such as fluorine (F) atom,^{44,45} chlorine (Cl) atom,⁴⁶ and ester groups⁴⁷ are usually introduced to these polymers in pursuit of a deep-lying HOMO level and high open-circuit voltage (V_{oc}). Specifically, F atom is most widely used to modulate the energy levels of polymer donors (Scheme 1). For example, Xue *et al.* simultaneously fluorinated thiophene rings in the π -bridge and side chains to synthesize polymer J91 with low HOMO energy level.⁴⁴ The OSCs based on J91:*m*-ITIC blend film showed a high V_{oc} of 0.984 V, which was 0.284 V higher than that of the non-fluorinated counterpart. Besides, F atom was used synergistically with other electron-withdrawing substituents, such as ester group,⁴⁷ to downshift the energy levels of polymer donors. A high efficiency of 17.3% was achieved based on a highly fluorinated polymer donor PTzBI-dF with a low ΔE_3 of 0.21 V.⁴⁵ However, fluorination will increase the complexity of synthesis and require the use of high-risk reagents. Therefore, it is of critical importance to design new polymer donors with deep-lying HOMO levels and high device performance *via* facile synthesis for application in OSCs. This point was also highlighted by a recent work of Hou's group, where suitable energy levels and high device performance were obtained by an easily synthesized poly(thiophene vinylene) derivative with ester group substitution.⁴⁸

Recently, we demonstrated that 3,4-dicyanothiophene (DCT) is a promising electron-deficient building block with structural simplicity and synthetic accessibility.⁴⁹ The DCT-based polymers exhibited deep-lying HOMO level, and favorable face-on orientation and fibril-assembly in films.^{49,50} In addition, the large dipole moment caused by cyano-group can induce a higher relative dielectric constant, which may reduce the exciton binding energy and charge recombination losses.^{51,52} Herein, we introduced DCT unit into the benchmark polymer benzo[1,2-*b*:4,5-*b'*]dithiophene (BDT)-*alt*-benzo[1,2-*c*:4,5-*c'*]dithiophene-4,8-dione (PBDB-TF)⁵³ as the third comonomer to form a set of random ternary copolymers for application in OSCs. The DCT-based ternary copolymers showed gradually down-shifted HOMO levels with the increase of DCT content as compared to PBDB-TF. When blended with the non-fullerene acceptor Y6-BO,⁵⁴ the terpolymer PFBCNT20 yielded a high PCE of 16.3% due to the enhanced V_{oc} and lower non-radiative recombination energy loss (0.23 eV). A further enhanced PCE of 16.6% was achieved by the ternary OSC of PFBCNT20:Y6-BO:PC₇₁BM with a smaller non-radiation energy loss of 0.22 eV. These results show that the introduction of DCT unit as the third comonomer is an easy and effective strategy to develop high-performance polymer donors with reduced energy loss and increased V_{oc} for OSCs.

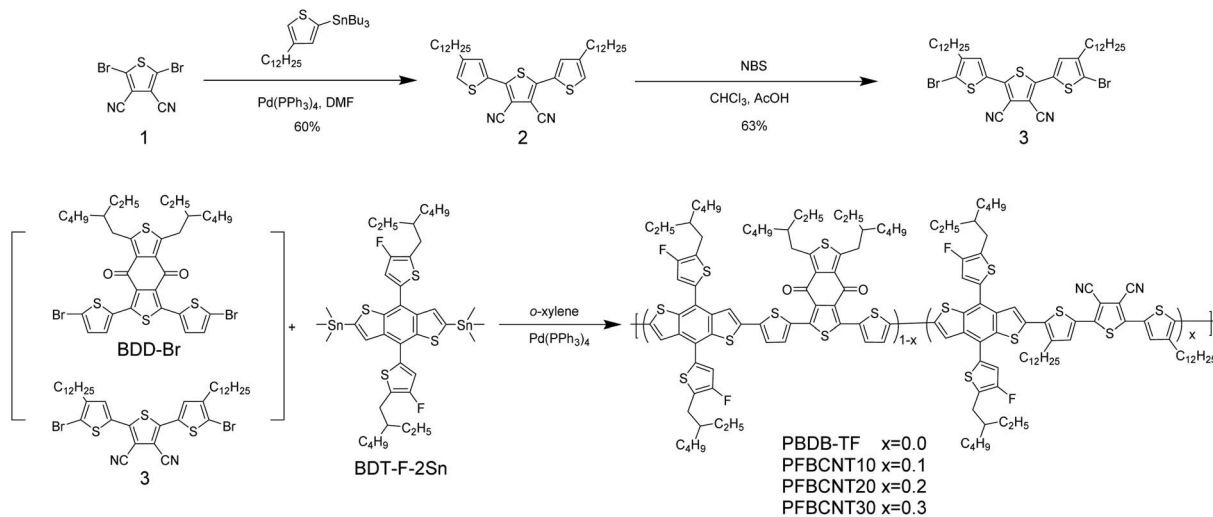
Results and discussion

Polymer synthesis

The synthesis route of the polymers was exhibited in Scheme 2. Detailed procedures for the synthesis of monomer 3 and the



Scheme 1 Molecular structures of representative polymer donors with deep-lying HOMO levels.



Scheme 2 The synthesis route and chemical structures of the polymers PFBCNT_x.

polymers can be found in the ESI.† The synthesis of monomer 3 started from precursor 1, which was obtained following previously reported procedures.⁴⁹ The compound 2 can be achieved by Stille coupling between the precursor 1 and 2-(tri-*n*-butylstannyl)-4-dodecylthiophene. Then bromination on compound 2 with *N*-bromosuccinimide (NBS) generated the monomer 3. The nuclear magnetic resonance (NMR) spectra of molecules 2 and 3 were shown in Fig. S1–S4.† The polymers were obtained *via* Stille polymerization. The number-average molecular weight (M_n) and molar-mass dispersity ($D_M = M_w/M_n$) of the polymers were measured by gel permeation chromatography in 1,2,4-trichlorobenzene at 140 °C. The results are shown in Table 1. It is worth mentioning that the molecular weights of the DCT-containing random copolymers are comparable to the reference polymer PBDB-TF, which can mitigate the impact of molecular weight on the device performance.

Optical and electrochemical properties

The normalized UV-Vis absorption spectra of PBDB-TF and PFBCNT_x in chlorobenzene solution and thin films were shown in Fig. S5a† and 1b, respectively. The relevant numerical data was listed in Table 1. From solution to solid state, the absorption spectra of all the polymers slightly red-shifted. Similar optical bandgaps (E_g^{opt}) of 1.83 eV were calculated from the onsets of the absorption spectra in films. The films of the

polymers show strong absorption in the range of 400–700 nm, which form a good complementary absorption with the acceptor Y6-BO. The temperature dependent absorption spectra of the copolymers in diluted chlorobenzene solution were also recorded (Fig. S6†) to investigate the effect of DCT on the aggregation characteristics of the polymers. The reference polymer PBDB-TF and the three DCT-containing polymers showed similar temperature-dependent aggregation behavior. The strong vibronic 0–0 peak (λ_{0-0}) was gradually weakened when the solution temperature increased from room temperature to 95 °C, but the polymers are not completely unfolded even at 95 °C.

The HOMO levels of the polymers and the LUMO level of Y6-BO were measured by square wave voltammetry (SWV) from the onsets of the redox waves. The energy levels are reported relative to the energy level of ferrocene (Fc/Fc^+) of -5.13 eV *versus* vacuum.⁵⁵ The LUMO levels of the polymers and the HOMO level of Y6-BO were estimated using the E_g^{opt} . The relevant results were described in Fig. 1c and S5b (ESI†). Their numerical data was summarized in Table 1. The HOMO/LUMO level of PBDB-TF is $-5.48/-3.65$ eV. Compared to the reference polymer PBDB-TF, the HOMO energy levels of PFBCNT_x were down-shifted gradually upon increasing DCT content, which is -5.49 eV for PFBCNT10, -5.50 eV for PFBCNT20, and -5.53 eV for PFBCNT30, respectively. The LUMO energy levels of PFBCNT_x were also down-shifted with the increase of DCT content. The down-shifted energy levels were caused by the

Table 1 Molecular weights, optical properties, and energy levels of the polymers

Polymer	M_n (kDa)	D_M	λ_{max}^a (nm)	$E_g^{\text{opt}b}$ (eV)	HOMO ^c (eV)	LUMO ^d (eV)
PBDB-TF	36.3	2.2	618	1.83	-5.48	-3.65
PFBCNT10	43.3	2.1	618	1.83	-5.49	-3.66
PFBCNT20	49.5	2.4	618	1.83	-5.50	-3.67
PFBCNT30	48.0	2.0	618	1.83	-5.53	-3.70

^a Obtained from the polymer films. ^b E_g^{opt} (eV) = $1240/\lambda_{\text{onset}}$ (nm). ^c HOMO = $-(5.13 + E_{\text{ox}} - E_{\text{Fc}/\text{Fc}^+})$. ^d LUMO = HOMO + E_g^{opt} .

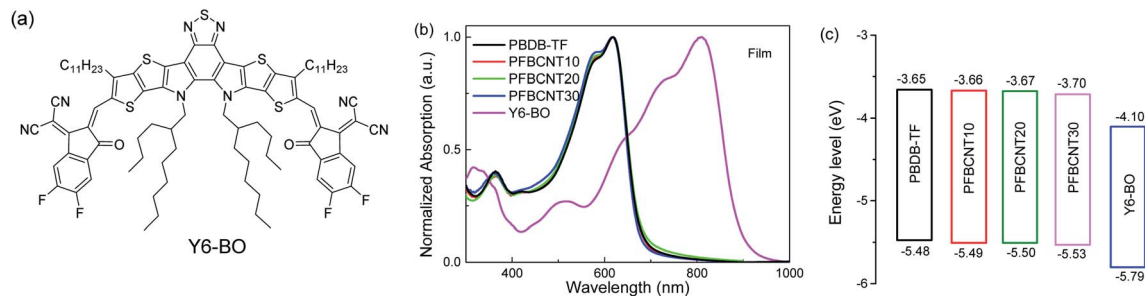


Fig. 1 (a) Chemical structure of the acceptor Y6-BO. (b) Normalized absorption spectra of PBDB-TF, PFBCNTx and Y6-BO in thin films. (c) Energy level diagrams of the donor and acceptor materials.

strong electron-withdrawing ability of cyano-group in DCT.⁴⁹ The energy levels of these polymers match well with the acceptor Y6-BO (HOMO/LUMO = $-5.79/-4.10$ eV). Thus, higher V_{oc} and lower E_{loss} are expectable in the resulting OSCs for the DCT-based polymers with respect to PBDB-TF.

Photovoltaic properties

The photovoltaic properties of the polymers were studied with a device architecture of glass/indium tin oxide/poly(3,4-ethylenedioxythiophene):poly(styrenesulfonate) (PEDOT:PSS)/PFBCNTx:Y6-BO/PDINO/Al, where PDINO is a perylene diimide derivative-functionalized amino N-oxide.⁵⁶ Device optimization was conducted in terms of the active layer thickness, polymers : Y6-BO weight ratio, solvent additive, thermal annealing at different temperatures, types of the electron transport layer and cathode. The photovoltaic parameters under various conditions

are shown in Fig. S7, S8 and Tables S1–S7.[†] The optimized devices for all polymers were obtained with chloroform as the host solvent, 1,8-diiodooctane (DIO) as the additive, and thermal annealing at 100 °C for 10 minutes. The optimal electron transport material was PDINO, and the cathode was Al electrode. As exhibited in Fig. 2a and Table 2, the optimal PBDB-TF:Y6-BO device showed a PCE of 15.7% with a V_{oc} of 0.81 V, a J_{sc} of 26.0 mA cm^{-2} , and an FF of 0.745. In contrast, the PFBCNT10:Y6-BO device showed a lower PCE of 14.9% with a reduced J_{sc} (25.7 mA cm^{-2}) and FF (0.710), but a slightly enhanced V_{oc} (0.82 V). The champion cell is achieved by PFBCNT20, which exhibited a PCE of 16.3% with a V_{oc} of 0.84 V, a J_{sc} of 26.3 mA cm^{-2} and an FF of 0.739. When the content of DCT is further increased to 30%, the performance of the PFBCNT30:Y6-BO device dropped to 13.9% due to the simultaneously reduced J_{sc} and FF values (23.9 mA cm^{-2} and 0.685,

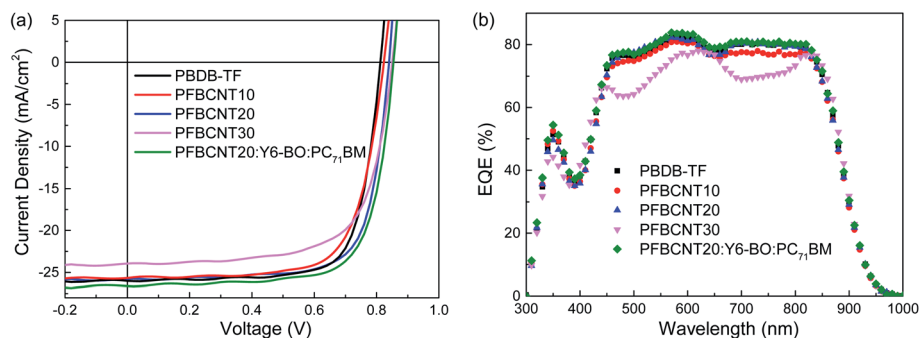


Fig. 2 (a) Current density–voltage (J – V) plots of the OSCs based on polymer:Y6-BO binary and PFBCNT20:Y6-BO:PC₇₁BM ternary blends under the illumination of AM1.5G, 100 mW cm^{-2} , and (b) EQE curves of the corresponding OSCs.

Table 2 Device parameters of the OSCs based on PBDB-TF and PFBCNTx under AM1.5G illumination (100 mW cm^{-2})

Donor	V_{oc} (V)	J_{sc} (mA cm^{-2})	$J_{sc,EQE}^c$ (mA cm^{-2})	FF	PCE (%)
PBDB-TF ^a	0.81 (0.81 ± 0.01)	26.0 (25.5 ± 0.7)	25.0	0.745 (0.747 ± 0.013)	15.7 (15.3 ± 0.4)
PFBCNT10 ^a	0.82 (0.82 ± 0.01)	25.7 (25.2 ± 0.3)	24.5	0.710 (0.707 ± 0.006)	14.9 (14.6 ± 0.3)
PFBCNT20 ^a	0.84 (0.84 ± 0.01)	26.3 (25.6 ± 0.2)	25.3	0.739 (0.738 ± 0.003)	16.3 (16.1 ± 0.2)
PFBCNT30 ^a	0.85 (0.85 ± 0.01)	23.9 (23.5 ± 0.3)	22.8	0.685 (0.686 ± 0.009)	13.9 (13.7 ± 0.2)
PFBCNT20 ^{a,b}	0.85 (0.84 ± 0.01)	26.6 (26.5 ± 0.1)	25.6	0.728 (0.73 ± 0.005)	16.6 (16.4 ± 0.2)

^a The data in brackets are the average values and standard deviation of at least 10 independent devices for each polymer:Y6-BO blend. ^b The ternary OSCs based on PFBCNT20:Y6-BO:PC₇₁BM blend film. ^c $J_{sc,EQE}$ represents the integrated current density obtained from EQE spectra.

respectively). It is noticed that the V_{oc} increases with the increased content of DCT, which is consistent with the HOMO levels of the polymers. The main reason for the increased V_{oc} could be assigned to the suppressed non-radiative energy loss, which will be discussed later. The external quantum efficiency (EQE) spectra of the optimized devices were shown in Fig. 2b. Due to the similar optical bandgap, all devices display a similar photo-response in the region from 300 to 950 nm. The OSCs based on PBDB-TF, PFBCNT10, and PFBCNT20 exhibited comparably high EQEs, consistent with the similar J_{sc} of the OSCs. These results evidenced that efficient charge generation can be maintained upon decreasing energy loss. The EQEs of the PFBCNT30-based solar cell is considerably lower than those of the other devices, which might be caused by the inferior morphological characteristics. To further improve the device performance, we introduced PC₇₁BM as the third component to the PFBCNT20:Y6-BO binary blend. The results are shown in Table S8,† Fig. 2, and Table 2. A higher PCE of 16.6% was successfully achieved by the PFBCNT20:Y6-BO:PC₇₁BM (1:1:0.2) device owing to the enhancement of V_{oc} (0.85 V) and J_{sc} (26.6 mA cm⁻²) with respect to the PFBCNT20:Y6-BO binary solar cell.

Blend morphology

Atomic force microscopy (AFM) and transmission electron microscopy (TEM) were used to investigate the effects of DCT on the blend morphological characteristics. As shown in Fig. S9,† the PBDB-TF:Y6-BO blend films exhibit uniform and smooth

surface morphology with a root-mean-square (RMS) roughness of 0.98 nm. The RMS roughness increased slightly to ≈ 1.3 nm with the introduction of DCT into the polymer donors. Bicontinuous interpenetrating networks with fibrillar structures and proper domain size were formed in the blends based on different polymers, which is favorable for efficient charge generation and transport.⁵⁷ These results suggest that the introduction of DCT unit does not influence the phase separation behavior of the donor:acceptor blends.

Therefore, the packing structures of the polymers in both neat films and donor:acceptor active layers were studied by grazing-incidence wide-angle X-ray scattering (GIWAXS) to understand the different J_{sc} and FF of the OSCs. As shown in Fig. S10 (ESI†), the PBDB-TF and PFBCNT x neat films demonstrate a preferential face-on orientation, which is beneficial for charge transport in the vertical direction. In blended films, the face-on orientation was retained for all the polymers (Fig. 3). The intensity of (010) diffraction in out-of-plane (OOP) direction increased from PBDB-TF to PFBCNT10 and PFBCNT20, which is consistent with the fact that the DCT unit can induce stronger interchain interaction and higher polymer crystallinity.⁴⁹ However, further increasing the content of DCT unit led to lower (010) diffraction intensity for PFBCNT30, which can be ascribed to the reduced regioregularity of PFBCNT30. The PFBCNT20:Y6-BO blend shows the strongest (010) diffraction in OOP direction, indicating an improved face-on orientation as compared to the other blends. For a quantitative analysis, the pole figures of the (100) stacking peaks of blended films are

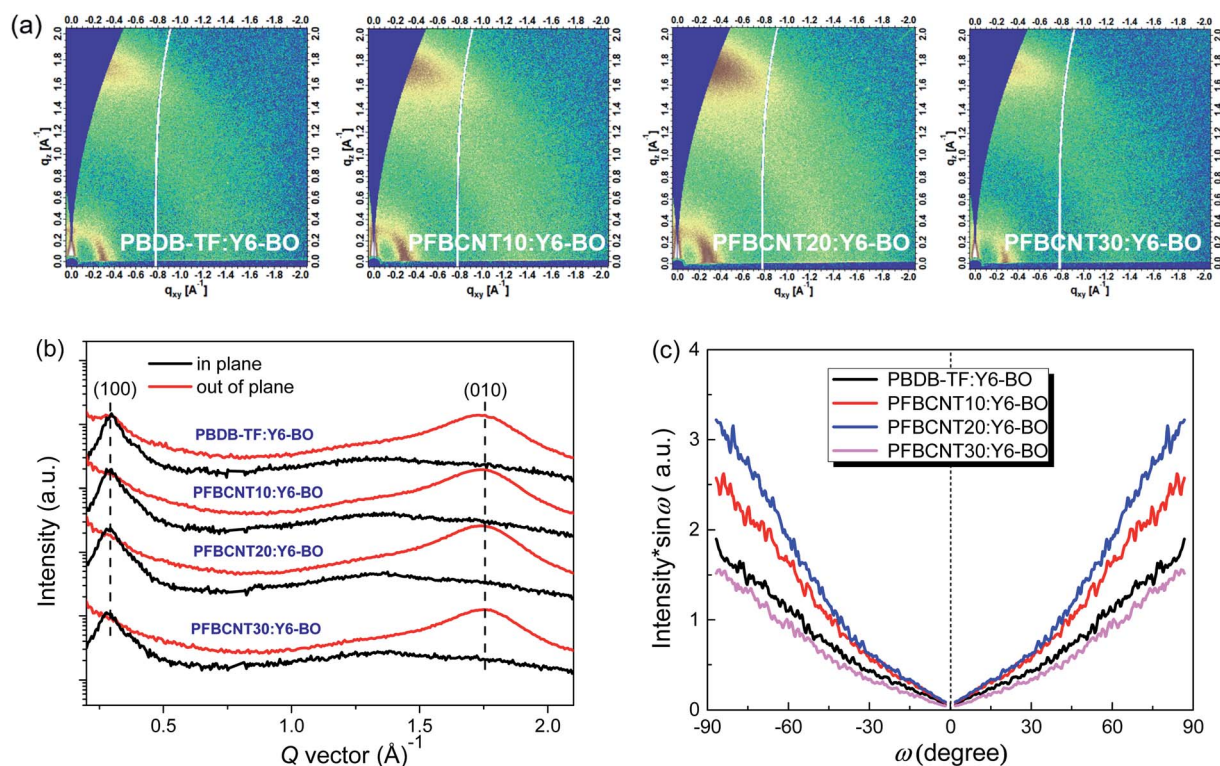


Fig. 3 (a) Two-dimensional GIWAXS patterns, (b) one-dimensional in-plane (IP) and out-of-plane (OOP) profiles and (c) pole figure of (100) peak for the polymers:Y6-BO blend films. Here ω is the polar angle of (100) peak.

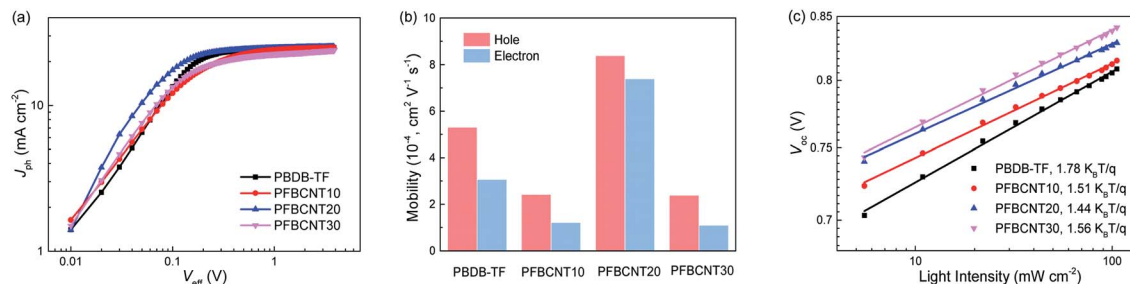


Fig. 4 (a) J_{ph} as a function of V_{eff} of the donor:acceptor binary OSCs based on PBDB-TF and PFBCNTx. (b) Hole and electron mobilities of the polymer:Y6-BO blends acquired from single-carrier devices. (c) V_{oc} as a function of P_{light} of the donor:acceptor binary OSCs based on PBDB-TF and PFBCNTx.

shown in Fig. 3c. The PFBCNT20:Y6-BO blend shows the highest face-on/edge-on ratio (12.7) and the largest face-on fraction (44%). The improved face-on orientation of molecules is beneficial to OOP charge transport and device performance of OSCs. As a result, the OSC based on PFBCNT20:Y6-BO blend exhibited the high J_{sc} and FF.

Charge transport, recombination, and extraction characteristics

The photoluminescence (PL) quenching experiments were conducted to investigate the charge generation and transfer at the interfaces between donor and acceptor of OSCs. As shown in Fig. S11 and Table S11,† all the PFBCNTx:Y6-BO blends exhibited over 98% PL quenching efficiency, indicating the efficient charge transfer in the blend films. Among them, the PFBCNT20:Y6-BO blend displayed the highest PL quenching efficiency (99.2%), suggesting the most efficient photo-induced charge transfer at the donor:acceptor interfaces of PFBCNT20:Y6-BO blend. The photocurrent density (J_{ph}) is plotted as a function of the effective voltage (V_{eff}) for all optimized devices (Fig. 4a) to study the charge generation of the OSCs.⁵⁸ J_{ph} is given by $J_{ph} = J_L - J_D$, where J_L and J_D are the current densities tested under illumination and in the dark, respectively. V_{eff} is defined as $V_{eff} = V_0 - V_{app}$, where V_0 and V_{app} are the voltage at $J_{ph} = 0$ and applied bias voltage, respectively. For the PFBCNT20:Y6-BO device, J_{ph} quickly saturated at a low V_{eff} of 0.2–0.3 V. And the calculated exciton dissociation probability ($P(E, T)$) under the maximum power

output condition are 90.3%, 87.0%, 95.2%, and 82.4% for the OSCs based on PBDB-TF, PFBCNT10, PFBCNT20, and PFBCNT30, respectively. These results further confirmed that the exciton dissociation and charge extraction are the most efficient in the PFBCNT20-based solar cell.

The hole and electron mobilities of the neat polymers and polymer:Y6-BO blends were measured by fitting the data acquired from single-carrier devices to the space-charge limited-current model (Fig. S12–S14, and Tables S12–S14, ESI†).⁵⁹ The neat film of PFBCNT20 exhibited a hole mobility of 2.08×10^{-3} cm² V⁻¹ s⁻¹, which is the highest one among the four polymers (Table S12†). In blends the highest hole mobility (μ_h) and electron mobility (μ_e) were also achieved by the PFBCNT20:Y6-BO blend (Fig. 4b), which are 8.39×10^{-4} and 7.40×10^{-4} cm² V⁻¹ s⁻¹, respectively. The high and balanced charge transport characteristic ($\mu_e/\mu_h = 0.88$) in the PFBCNT20:Y6-BO blend could effectively reduce charge carrier recombination, and thus giving high FF for the resulting OSC.

Moreover, the relationships of J_{sc} and V_{oc} as a function of the light intensity (P_{light}) were analyzed to investigate the recombination mechanisms of the OSCs.^{60–62} The J_{sc} as a function of light intensity (P_{light}) was plotted to investigate the bimolecular recombination. The relationship between J_{sc} and P_{light} can be described by $J_{sc} \propto (P_{light})^\alpha$, where α is the exponential factor. As shown in Fig. S15,† the α values of the optimized solar cells based on the four polymers are all close to unity, indicating negligible bimolecular recombination at short-circuit conditions in these devices. The correlation of V_{oc} and P_{light} can be described by the formula $V_{oc} \propto nkT/q \ln(P_{light})$, where k , T , and q

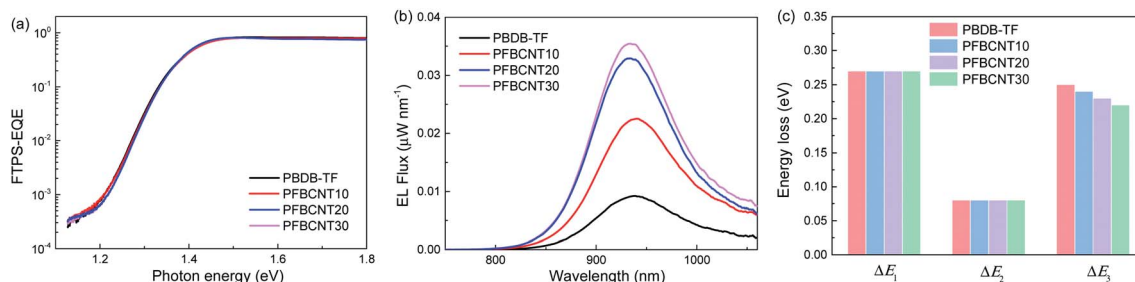


Fig. 5 (a) FTPS-EQE spectra, (b) EQE_{EL} spectra, and (c) detailed energy losses of the donor:acceptor binary OSCs based on PBDB-TF and PFBCNTx.

Table 3 Detailed energy losses of the OSCs based on the PFBCNTx:Y6-BO blend films

Polymer	E_g (eV)	qV_{oc}^{SQ} (eV)	qV_{oc}^{rad} (eV)	EQE_{EL} (%)	ΔE_1 (eV)	ΔE_2 (eV)	ΔE_3 (eV)
PBDB-TF	1.41	1.14	1.06	5.0×10^{-3}	0.27	0.08	0.25
PFBCNT10	1.41	1.14	1.06	1.1×10^{-2}	0.27	0.08	0.24
PFBCNT20	1.41	1.14	1.06	1.4×10^{-2}	0.27	0.08	0.23
PFBCNT30	1.41	1.14	1.06	1.5×10^{-2}	0.27	0.08	0.22

denote the Boltzmann constant, absolute temperature, and elementary charge, respectively.⁵⁴ When the slope is close to kT/q , the bimolecular recombination is dominant. While the trap-assisted recombination or geminate recombination dominates when the slope is close to $2kT/q$. As shown in Fig. 4c, the OSCs based on PBDB-TF, PFBCNT10, PFBCNT20, and PFBCNT30 exhibit a slope of $1.78kT/q$, $1.51kT/q$, $1.44kT/q$, and $1.56kT/q$, respectively. The lowest slope suggests that the trap-assisted recombination and geminate recombination can be most efficiently suppressed in the solar cell of PFBCNT20. Overall, these results show that the OSCs based on PFBCNT20:Y6-BO blend exhibited efficient charge generation, high and balanced charge transport, and efficient charge extraction.

Energy loss analysis

Fourier-transform photocurrent spectroscopy (FTPS) and external quantum efficiency of electroluminescence (EQE_{EL}) measurements were used to analyze the ΔE_{loss} of the OSCs in detail. The results are shown in Fig. 5 and Table 3. The optical bandgaps of the solar cells (E_g^{PVs}) were extracted from the EQE spectra, which were calculated to be 1.41 eV for all the devices. As discussed above, the total energy loss can be split into three terms: radiative recombination caused ΔE_1 and ΔE_2 , and non-radiative recombination caused ΔE_3 . The OSCs based on PBDB-TF and PFBCNTx show the same ΔE_1 (0.27 eV). The FTPS-EQE spectra of the PFBCNTx:Y6-BO solar cells exhibited almost identical onsets (Fig. 5a), thus leading to a low ΔE_2 of 0.08 eV for all the devices. As discussed above, the ΔE_3 is given by $\Delta E_3 = -kT \ln(EQE_{EL})$. Therefore, the EQE_{EL} spectra of the neat polymers and blend films were measured. As shown in Fig. S16,[†] the introduction of DCT has significantly enhanced the EQE_{EL} of the polymers from $1.3 \times 10^{-2}\%$ for PBDB-TF to $1.3 \times 10^{-1}\%$ for PFBCNT30, implying that the DCT-containing polymers are more emissive and will have lower non-radiative recombination losses in the resulting OSCs. The EQE_{EL} spectra of the blend films are shown in Fig. 5b and the numerical data are listed in Table 3. Similar enhancement of EQE_{EL} was also observed. The PBDB-TF:Y6-BO-based device showed an EQE_{EL} of $5.0 \times 10^{-3}\%$, while the PFBCNT30:Y6-BO-based device produced a much higher EQE_{EL} of $1.5 \times 10^{-2}\%$. As a result, the lowest ΔE_3 of 0.22 eV was found in PFBCNT30:Y6-BO-based device, which is lower than that of PBDB-TF:Y6-BO by 30 meV. Fig. 5c shows the comparison of radiative and nonradiative energy losses of the OSCs based on PBDB-TF and PFBCNTx. Clearly, the introduction of DCT unit into the polymer backbone has led to monotonically reduced ΔE_3 . And the reduced ΔE_3 is the major reason for the lower ΔE_{loss} and higher V_{oc} of the resulting OSCs.

Conclusions

In summary, three random ternary copolymers were prepared with deeper HOMO levels by introducing DCT units into PBDB-TF. The non-radiative energy loss in solar cells were suppressed as a result of the down-shifted HOMO level of the polymer donors upon introducing DCT units. The solar cell with a higher PCE was achieved by PFBCNT20 as compared to the reference polymer PBDB-TF, which is mainly caused by the enhanced V_{oc} , suppressed non-radiative energy loss, and improved face-on orientation. After introducing PC₇₁BM as the third component, the ternary solar cell of PFBCNT20:Y6-BO:PC₇₁BM yielded a high PCE of 16.6%. Our work proves that the introduction of DCT units into donor polymers is an easy and feasible strategy to improve device performance of OSCs *via* decreasing the non-radiative energy loss.

Conflicts of interest

There are no conflicts to declare.

Acknowledgements

The research was financially supported by the Ministry of Science and Technology of China (2019YFA0705900 and 2017YFA0206600), National Natural Science Foundation of China (U20A6002, 21875072, 51703172, and 51973169), Guangdong Innovative and Entrepreneurial Research Team Program (2019ZT08L075), Beijing National Laboratory for Molecular Sciences (BNLMS201901), and the Fundamental Research Funds for the Central Universities (South China University of Technology, No. D2190310).

References

- J. Hou, O. Inganäs, R. H. Friend and F. Gao, *Nat. Mater.*, 2018, **17**, 119–128.
- P. Cheng, G. Li, X. Zhan and Y. Yang, *Nat. Photonics*, 2018, **12**, 131–142.
- Y. Li, G. Xu, C. Cui and Y. Li, *Adv. Energy Mater.*, 2018, **8**, 1701791.
- Y. Zhang, C. Duan and L. Ding, *Sci. Bull.*, 2020, **65**, 2040–2042.
- Y. Lin, J. Wang, Z. Zhang, H. Bai, Y. Li, D. Zhu and X. Zhan, *Adv. Mater.*, 2015, **27**, 1170–1174.
- Z. Xiao, X. Jia, D. Li, S. Wang, X. Geng, F. Liu, J. Chen, S. Yang, T. P. Russell and L. Ding, *Sci. Bull.*, 2017, **62**, 1494–1496.

- 7 J. Yuan, Y. Zhang, L. Zhou, G. Zhang, H. Yip, T. Lau, X. Lu, C. Zhu, H. Peng, P. Johnson, M. Leclerc, Y. Cao, J. Ulanski, Y. Li and Y. Zou, *Joule*, 2019, **3**, 1140–1151.
- 8 C. Duan and L. Ding, *Sci. Bull.*, 2020, **65**, 1231–1233.
- 9 S. Zhang, Y. Qin, J. Zhu and J. Hou, *Adv. Mater.*, 2018, **30**, 1800868.
- 10 Q. Liu, Y. Jiang, K. Jin, J. Qin, J. Xu, W. Li, J. Xiong, J. Liu, Z. Xiao, K. Sun, S. Yang, X. Zhang and L. Ding, *Sci. Bull.*, 2020, **65**, 272–275.
- 11 C. Sun, F. Pan, H. Bin, J. Zhang, L. Xue, B. Qiu, Z. Wei, Z. Zhang and Y. Li, *Nat. Commun.*, 2018, **9**, 743.
- 12 C. Duan and L. Ding, *Sci. Bull.*, 2020, **65**, 1422–1424.
- 13 C. Duan and L. Ding, *Sci. Bull.*, 2020, **65**, 1597–1599.
- 14 R. Yu, H. Yao, L. Hong, Y. Qin, J. Zhu, Y. Cui, S. Li and J. Hou, *Nat. Commun.*, 2018, **9**, 4645.
- 15 X. Xu, L. Yu, H. Yan, R. Li and Q. Peng, *Energy Environ. Sci.*, 2020, **13**, 4381–4388.
- 16 K. Weng, L. Ye, L. Zhu, J. Xu, J. Zhou, X. Feng, G. Lu, S. Tan, F. Liu and Y. Sun, *Nat. Commun.*, 2020, **11**, 2855.
- 17 L. Ye, H. Hu, M. Ghasemi, T. Wang, B. A. Collins, J.-H. Kim, K. Jiang, J. H. Carpenter, H. Li, Z. Li, T. McAfee, J. Zhao, X. Chen, J. L. Y. Lai, T. Ma, J.-L. Bredas, H. Yan and H. Ade, *Nat. Mater.*, 2018, **17**, 253–260.
- 18 S. Athanasopoulos, F. Schauer, V. Nádaždy, M. Weiß, F. J. Kahle, U. Scherf, H. Bässler and A. Köhler, *Adv. Energy Mater.*, 2019, **9**, 1900814.
- 19 R. Gurney, D. Lidzey and T. Wang, *Rep. Prog. Phys.*, 2019, **82**, 036601.
- 20 A. Classen, C. L. Chochos, L. Lüer, V. G. Gregoriou, J. Wortmann, A. Osvet, K. Forberich, I. McCulloch, T. Heumüller and C. J. Brabec, *Nat. Energy*, 2020, **5**, 711–719.
- 21 J. Qin, L. Zhang, C. Zuo, Z. Xiao, Y. Yuan, S. Yang, F. Hao, M. Cheng, K. Sun, Q. Bao, Z. Bin, Z. Jin and L. Ding, *J. Semicond.*, 2021, **42**, 010501.
- 22 L. Zhan, S. Li, X. Xia, Y. Li, X. Lu, L. Zuo, M. Shi and H. Chen, *Adv. Mater.*, 2021, **33**, 2007231.
- 23 M. Green, E. Dunlop, J. Hohl-Ebinger, M. Yoshita, N. Kopidakis and X. Hao, *Prog. Photovolt: Res. Appl.*, 2020, **28**, 629–638.
- 24 S. M. Menke, N. A. Ran, G. C. Bazan and R. H. Friend, *Joule*, 2018, **2**, 25–35.
- 25 D. Qian, Z. Zheng, H. Yao, W. Tress, T. R. Hopper, S. Chen, S. Li, J. Liu, S. Chen, J. Zhang, X. K. Liu, B. Gao, L. Ouyang, Y. Jin, G. Pozina, I. A. Buyanova, W. M. Chen, O. Inganas, V. Coropceanu, J. L. Bredas, H. Yan, J. Hou, F. Zhang, A. A. Bakulin and F. Gao, *Nat. Mater.*, 2018, **17**, 703–709.
- 26 J. Yuan, H. Zhang, R. Zhang, Y. Wang, J. Hou, M. Leclerc, X. Zhan, F. Huang, F. Gao, Y. Zou and Y. Li, *Chem*, 2020, **6**, 2147–2161.
- 27 S. Li, L. Zhan, Y. Jin, G. Zhou, T. Lau, R. Qin, M. Shi, C. Li, H. Zhu, X. Lu, F. Zhang and H. Chen, *Adv. Mater.*, 2020, **32**, 2001160.
- 28 J. Yao, T. Kirchartz, M. S. Vezie, M. A. Faist, W. Gong, Z. He, H. Wu, J. Troughton, T. Watson, D. Bryant and J. Nelson, *Phys. Rev. Appl.*, 2015, **4**, 014020.
- 29 S. M. Menke, A. Cheminal, P. Conaghan, N. A. Ran, N. C. Greehnam, G. C. Bazan, T.-Q. Nguyen, A. Rao and R. H. Friend, *Nat. Commun.*, 2018, **9**, 277.
- 30 J. Dang, Z. Yang, W. Guo, J. Dou, H. Wang and M. Wang, *J. Phys. Chem. Lett.*, 2020, **11**, 8100–8107.
- 31 D. Baran, T. Kirchartz, S. Wheeler, S. Dimitrov, M. Abdelsamie, J. Gorman, R. S. Ashraf, S. Holliday, A. Wadsworth, N. Gasparini, P. Kaienburg, H. Yan, A. Amassian, C. J. Brabec, J. R. Durrant and I. McCulloch, *Energy Environ. Sci.*, 2016, **9**, 3783–3793.
- 32 X. Liu, X. Du, J. Wang, C. Duan, X. Tang, T. Heumueller, G. Liu, Y. Li, Z. Wang, J. Wang, F. Liu, N. Li, C. J. Brabec, F. Huang and Y. Cao, *Adv. Energy Mater.*, 2018, **8**, 1801699.
- 33 N. An, Y. Cai, H. Wu, A. Tang, K. Zhang, X. Hao, Z. Ma, Q. Guo, H. S. Ryu, H. Y. Woo, Y. Sun and E. Zhou, *Adv. Mater.*, 2020, **32**, 2002122.
- 34 C. Wolff, P. Caprioglio, M. Stolterfoht and D. Neher, *Adv. Mater.*, 2019, **31**, 1902762.
- 35 D. Luo, R. Su, W. Zhang, Q. Gong and R. Zhu, *Nat. Rev. Mater.*, 2020, **5**, 44–60.
- 36 K. Vandewal, Z. Ma, J. Bergqvist, Z. Tang, E. Wang, P. Henriksson, K. Tvingstedt, M. R. Andersson, F. Zhang and O. Inganäs, *Adv. Funct. Mater.*, 2012, **22**, 3480–3490.
- 37 Y. Cui, H. Yao, J. Zhang, T. Zhang, Y. Wang, L. Hong, K. Xian, B. Xu, S. Zhang, J. Peng, Z. Wei, F. Gao and J. Hou, *Nat. Commun.*, 2019, **10**, 2515.
- 38 L. Zhang, X. Huang, C. Duan, Z. Peng, L. Ye, N. Kirby, F. Huang and Y. Cao, *J. Mater. Chem. A*, 2021, **9**, 556–565.
- 39 B. Gao, H. Yao, L. Hong and J. Hou, *Chin. J. Chem.*, 2019, **37**, 1153–1157.
- 40 J. Liu, S. Chen, D. Qian, B. Gautam, G. Yang, J. Zhao, J. Bergqvist, F. Zhang, W. Ma, H. Ade, O. Inganäs, K. Gundogdu, F. Gao and H. Yan, *Nat. Energy*, 2016, **1**, 16089.
- 41 Z. Zheng, O. M. Awartani, B. Gautam, D. Liu, Y. Qin, W. Li, A. Bataller, K. Gundogdu, H. Ade and J. Hou, *Adv. Mater.*, 2017, **29**, 1604241.
- 42 S. Chen, Y. Wang, L. Zhang, J. Zhao, Y. Chen, D. Zhu, H. Yao, G. Zhang, W. Ma, R. H. Friend, P. C. Y. Chow, F. Gao and H. Yan, *Adv. Mater.*, 2018, **30**, 1804215.
- 43 S. Li, L. Zhan, C. Sun, H. Zhu, G. Zhou, W. Yang, M. Shi, C. Li, J. Hou, Y. Li and H. Chen, *J. Am. Chem. Soc.*, 2019, **141**, 3073–3082.
- 44 L. Xue, Y. Yang, J. Xu, C. Zhang, H. Bin, Z. Zhang, B. Qiu, X. Li, C. Sun, L. Gao, J. Yao, X. Chen, Y. Yang, M. Xiao and Y. Li, *Adv. Mater.*, 2017, **29**, 1703344.
- 45 B. Fan, M. Li, D. Zhang, W. Zhong, L. Ying, Z. Zeng, K. An, Z. Huang, L. Shi, G. C. Bazan, F. Huang and Y. Cao, *ACS Energy Lett.*, 2020, **5**, 2087–2094.
- 46 H. Yao, J. Wang, Y. Xu, S. Zhang and J. Hou, *Acc. Chem. Res.*, 2020, **53**, 822–832.
- 47 H. Sun, T. Liu, J. Yu, T. K. Lau, G. Zhang, Y. Zhang, M. Su, Y. Tang, R. Ma, B. Liu, J. Liang, K. Feng, X. Lu, X. Guo, F. Gao and H. Yan, *Energy Environ. Sci.*, 2019, **12**, 3328–3337.
- 48 J. Ren, P. Bi, J. Zhang, J. Liu, J. Wang, Y. Xu, Z. Wei, S. Zhang and J. Hou, *Natl. Sci. Rev.*, 2021, **8**, nwab031.

- 49 B. Zhang, Y. Yu, J. Zhou, Z. Wang, H. Tang, S. Xie, Z. Xie, L. Hu, H. L. Yip, L. Ye, H. Ade, Z. Liu, Z. He, C. Duan, F. Huang and Y. Cao, *Adv. Energy Mater.*, 2020, **10**, 1904247.
- 50 B. Zhang, Y. Yu, Z. Liu, X. Liu, C. Duan and F. Huang, *Acta Polym. Sin.*, 2020, **51**, 620–631.
- 51 X. Liu, B. Xie, C. Duan, Z. Wang, B. Fan, K. Zhang, B. Lin, F. J. M. Colberts, W. Ma, R. A. J. Janssen, F. Huang and Y. Cao, *J. Mater. Chem. A*, 2018, **6**, 395–403.
- 52 L. J. A. Koster, S. E. Shaheen and J. C. Hummelen, *Adv. Energy Mater.*, 2012, **2**, 1246–1253.
- 53 M. Zhang, X. Guo, W. Ma, H. Ade and J. Hou, *Adv. Mater.*, 2014, **26**, 1118–1123.
- 54 L. Hong, H. Yao, Z. Wu, Y. Cui, T. Zhang, Y. Xu, R. Yu, Q. Liao, B. Gao, K. Xian, H. Y. Woo, Z. Ge and J. Hou, *Adv. Mater.*, 2019, **31**, 1903441.
- 55 C. M. Cardona, W. Li, A. E. Kaifer, D. Stockdale and G. C. Bazan, *Adv. Mater.*, 2011, **23**, 2367–2371.
- 56 Z. Zhang, B. Qi, Z. Jin, D. Chi, Z. Qi, Y. Li and J. Wang, *Energy Environ. Sci.*, 2014, **7**, 1966–1973.
- 57 T. Xia, Y. Cai, H. Fu and Y. Sun, *Sci. China: Chem.*, 2019, **62**, 662–668.
- 58 P. W. M. Blom, V. D. Mihailetschi, L. J. A. Koster and D. E. Markov, *Adv. Mater.*, 2007, **19**, 1551–1566.
- 59 J. C. Blakesley, F. A. Castro, W. Kylberg, G. F. A. Dibb, C. Arantes, R. Valaski, M. Cremona, J. S. Kim and J. S. Kim, *Org. Electron.*, 2014, **15**, 1263–1272.
- 60 L. J. A. Koster, E. C. P. Smits, V. D. Mihailetschi and P. W. M. Blom, *Phys. Rev. B: Condens. Matter Mater. Phys.*, 2005, **72**, 085205.
- 61 S. R. Cowan, A. Roy and A. J. Heeger, *Phys. Rev. B: Condens. Matter Mater. Phys.*, 2010, **82**, 245207.
- 62 I. Riedel, J. Parisi, V. Dyakonov, L. Lutsen, D. Vanderzande and J. C. Hummelen, *Adv. Funct. Mater.*, 2004, **14**, 38–44.